IIETA International Information and Engineering Technology Association
Advancing the World of Information and Engineering

Annales de Chimie - Science des Matériaux
Vol. 48, No. 5, October, 2024, pp. 639-653
Journal homepage: http://iieta.org/journals/acsm

The Effect of Changing the Reinforcing Angle of a Composite Material on the Tensile and Compressive Resistance Using the ANSYS Program

Luqman Khaleel Hyder Alatrushi, Mohammad Takey Elias Kassim, Emad Toma Karash*, Waleed Mohammed Najm

Mechanical Technology Department, Technical Institute, Northern Technical University, Mosul 41000, Iraq

Corresponding Author Email: emadbane2007@ntu.edu.iq

https://doi.org/10.18280/acsm.480505

Received: 20 May 2024
Revised: 21 September 2024
Accepted: 29 September 2024
Available online: 29 October 2024

Keywords:
composite materials, deformation, fiber reinforced, impact test, tensile test, impact test

ABSTRACT

This work uses finite elements to build and examine composite laminates constructed of carbon fiber reinforced polymer (CFRP). The great strength compared to weight of composite materials is an important characteristic. Using the finite element method and the ANSYS program, the optimal resistance model for tensile testing and compressive testing was chosen. This article will present hybrid 3D simulation models of woven materials reinforced with fibers, with the goal of optimizing the model by adjustment of the reinforcement angle. The Math-Cad and ANSYS software will be used to compare these reinforced models from different angles in addition to testing them under compressive and tensile loads. The results of the tensile testing of the models were illustrated using von Mises stress theory of failure. Of all the models, the tenth is the one that is least susceptible to failure. The resistance to breakdown is weaker (51.5%) when compared to the resistance to the fifth model's breakdown. The von Mises stress theory of failure was used to illustrate the findings of the compressive testing of the models. The third model is the one that has the lowest failure probability. The resistance to collapse is significantly lower (48%) than the resistance to the fifth model's disintegration. Additionally, the results show that the sixth model had the lowest shear stress (1.5686 MPa), whereas the tenth model had the highest shear stress (22.734 MPa). For resistance to stresses, strains, and deformations caused by the tensile test and compression test, the third model is the best selection.

1. INTRODUCTION

In the world of engineering, fiber reinforced composite materials are becoming increasingly significant. These kinds of materials have a significant impact on many industrial sectors, particularly the aerospace industry, Additionally, a number of different industries, including the automotive, maritime, and medical sectors as well as the field of connections and transportation and in the construction and military field [1-4]. A substance made up of two or more components is referred to as a composite material. A matrix that holds the fiber in place and the fiber itself, which acts as reinforcement, are the two components of materials with fiber reinforcement. The examination of components made of such materials is a challenging process since they are composed of two quite distinct materials with very diverse properties [5]. There are two methods for researching the behavior of fiber-reinforced composite materials. The composite material is treated by the micro-mechanical technique as a blend of different materials, and the average properties are derived by taking into account the characteristics of each individual material within a unit-cell. The continuum method states that the composite material is homogeneous and has uniform average attributes [6, 7]. The advantages of polymeric composites over metals include greater fatigue strength, improved corrosion resistance, and reduced weight [8, 9]. When subjected to tension, flexural, and compression forces, polymeric composites are vulnerable to mechanical damage, which can result in material failure. As a result, it's important to utilize materials with better damage tolerance and to conduct a sufficient mechanical examination. By enhancing the interlinear characteristics of the matrix and reinforcing it with bidirectional woven fabrics, epoxy polymeric composites' damage tolerance can be increased [10, 11]. The tensile and compressive load resistance characteristics of two- and three-dimensional models are the subject of extensive investigation. A portion of this research involved designing various models with fibers of various sorts and orientations, while the remaining portion involved doing various trials with composite materials under various stresses [6, 12, 13]. A GHPFRC matrix composite combines reinforcing elements like mineral or inorganic non-mineral fibers, synthetic fibers, or natural organic fibers with matrix compounds like mortar, grout, or concrete. GHPFRC matrix composite is more flexible, low-carbon, cost-effective, and environmentally friendly than regular concrete [14]. The main emphasis of this experimental work was on the yield and tensile strength of composite materials made with varying proportions of pure jute and

chicken feather fiber. The group (A) including 95% pure jute fibers and 5% chicken feather fibers had the highest tensile strength among the four composite groups with relative differences, according to the obtained data [15]. The cantilever beam system under direct external load was the subject of the current study. It features holes of different shapes on its surface. The strain results show that the models made of composite materials are increasing at varying rates; the model made of glass fibers attained the highest values (92.18%) [16]. The tensile strength of the AA 2014 composite, which was created using the electromagnetic stir casting technology, is examined in this study in relation to the weight ratio of non-carbonated eggshell. It was found that the non-carbonated eggshell reinforcement in the AA 2014 aluminium alloy increased the hardness and tensile strength by 39.58% and 55.24%, respectively [17].

The present investigation examined the damage behavior of a composite material under the influence of axial tension, the stages of failure progression, the behavior of effective tensile elasticity in various compounds, and the progression of damage development and failure strength [11]. Banakar et al. [18] compared the performance of a three dimension orthogonal woven composite and a 3DAC in a semi-static three-point bending test. The outcomes demonstrated that various structural fabrics had an impact on the composite's flexural characteristics. In this investigation, the characteristics of industrial thermoplastics and selective laser sintering (SLS) are compared [19]. This suggests that when pressure is applied, mechanical qualities are increased in comparison to traditional approaches. The orientation and volume percentage of the fibers visibly affect the composites' mechanical characteristics. The article discusses how the thickness and fiber orientation of laminated polymer composites affect their tensile properties [20]. The materials are epoxy resin, which acts as a matrix and transfers load to stiff fibers by shear stress, and bi-woven fiber glass, which acts as reinforcement. Two different thicknesses (2 mm and 3 mm) and three alternative orientations (30°, 45°, and 90°) are taken into consideration. Using manual lay-up, the specimens are produced. A UTM machine is used to assess the specimens' tensile strength. They concluded that specimens with reduced thickness yield higher ultimate tensile strength, independent of fiber orientation. The sample elongation is larger at angles of 30° and decreased at angles of 90°, they finally concluded. Example descriptions of failures were analysed. The results showed consistent tensile failure and threads at 3DBAC that could bear the maximum stress. The investigation of the many forms of failures associated with lightweight composite materials led to the conclusion that these materials possess higher flexural strength capabilities. This finding provides a fundamental basis for the design and manufacturing of lightweight structures [21]. In this paper [22], the evolution of the impact in a composite laminate under stress is studied experimentally and numerically in ABAQUS/EXPRESS. X-ray tomography is used to study damage envelopes utilizing the NDE (Non Destructive Evaluation) approach. It has been found that the qualities of the constituent materials, layer orientations and stacking patterns, and plate thicknesses all affect the CAI's strength. In this work [23], modifications in the weight percentages of woven fibers (15, 25, and 35%) were used to analyze the mechanical and physical properties of epoxy resin composites reinforced with woven fibers and other unidirectional composites. This investigation showed that while the influence of other compounds rose, the tensile strength of the compound decreased as the weight of the woven fibers grew. Bending tests, which are conducted by placing a material under load and applying strain to bend it to failure, are the most popular experimental characterization method in the sector [24]. In order to examine structural defects in composite materials, this study reinforces the materials from several angles. The analysis's conclusions demonstrate that the fibers' orientation affects both K1LC and the maximum strength of failure. According to the findings, the composite material functions best when the fibers are arranged lengthwise in the direction of tensile strength [25]. This paper [26] discusses a novel technique to comprehend anisotropic fiber reinforced composite materials' failure mechanisms as a result of low velocity. The Impact Break method is used to examine how these composites' mechanical characteristics and failure processes relate to loading speed. In composite materials, the change from static to impact loading conditions is particularly notable. features that have been demonstrated by experiment. When the shock load is applied initially, composite materials damage is seen.

In this article, hybrid 3D simulation models of fiber-reinforced woven materials will be shown in order to provide the best model by modifying the angle of reinforcement. In addition to being tested under the influence of compressive and tensile loads, these reinforced models will also be compared between them from various angles using the Math-Cad and ANSYS software.

2. MATERIALS AND MODEL ANALYSIS

For each test, ten composite-material models are outfitted with various codes: The first ten models were used for tensile tests, and the second ten models were used for compression tests. The mechanical characteristics of the composite materials used in this article are shown in Table 1.

The reinforcements in composite materials are always orientated in the direction of the load. In cases when the load direction is non-perpendicular to the fibers and is varied, it is particularly crucial to assess the mechanical performance of the laminate. The codes in Table 2 were chosen in order to look at how fiber orientation affects tensile, compression, bending, and impact resistances. The results of the program Mathcad-15's analysis of the orthotropic mechanical properties of composite materials for the ten codes are also displayed in Table 2.

Table 1. Mechanical properties of carbon fiber and polyester [27]

Property	Modulus of Elasticity E, (GPa)	Modulus of Rigidity G, (GPa)	Density ρ, Kg/m^3	Poisons Ratio μ
Carbon fiber	400	108	1780	0.32
Polyester	4.4	1.633	1455	0.33

Table 2. The mathematical properties of composite materials as produced by Mathcad 15

Model	Materials	Codes	E_{ii}, GPa	G_{ij}, GPa	μ_{ij}
Model - 1	Carbon Fiber and Polyester Resin	$[0^{\circ}/90^{\circ}]_{10}$	E_{11}=134.3 E_{22}=134.3 E_{33}=23.26	G_{12}=6.153 G_{13}=5.134 G_{23}=5.134	μ_{12}=0.004 μ_{13}=0.333 μ_{23}=0.333
Model - 2		$[0^{\circ}/\pm30^{\circ}/90^{\circ}]_{5}$	E_{11}=133.8 E_{22}=78.77 E_{33}=23.19	G_{12}=28.93 G_{13}=5.416 G_{23}=4.853	μ_{12}=0.282 μ_{13}=0.242 μ_{23}=0.278
Model - 3		$[0^{\circ}/\pm45^{\circ}/90^{\circ}]_{5}$	E_{11}=94.74 E_{22}=94.74 E_{33}=23.26	G_{12}=36.52 G_{13}=5.134 G_{23}=5.134	μ_{12}=0.297 μ_{13}=0.058 μ_{23}=0.058
Model - 4		$[0^{\circ}/30^{\circ}/60^{\circ}/90^{\circ}/0^{\circ}/-30^{\circ}/-60^{\circ}/90^{\circ}/0^{\circ}/30^{\circ}/60^{\circ}/90^{\circ}/^{\circ}0°/-30°/-60°/90^{\circ}/0°/30°/60°/90^{\circ}]$	E_{11}=106.1 E_{22}=106.1 E_{33}=23.25	G_{12}=28.56 G_{13}=5.133 G_{23}=5.133	μ_{12}=0.202 μ_{13}=0.267 μ_{23}=0.267
Model - 5		$[0^{\circ}/30°/0^{\circ}/45^{\circ}/0/60^{\circ}/0^{\circ}/75°/0°/90°]_{2}$	E_{11}=142.4 E_{22}=61.51 E_{33}=22.8	G_{12}=16.4 G_{13}=5.46 G_{23}=4.757	μ_{12}=0.037 μ_{13}=0.323 μ_{23}=0.327
Model - 6		[90°/0°/10°/-15°/20°/-25°/30°/-35°/40°/-45°/50°/-55°/60°/-65°/70°/-75°/80°/-85°/0°/90°]	E_{11}=94.51 E_{22}=105.11 E_{33}=23.26	G_{12}=33.39 G_{13}=5.079 G_{23}=5.191	μ_{12}=0.246 μ_{13}=0.252 μ_{23}=0.243
Model - 7		[0°/90°/±10°/±20°/±30°/±40°/±50°/±60°/±70°/±80°/90°/0°]	E_{11}=99.71 E_{22}=99.71 E_{33}=23.26	G_{12}=33.49 G_{13}=5.134 G_{23}=5.134	μ_{12}=0.261 μ_{13}=0.248 μ_{23}=0.248
Model - 8		$[0^{\circ}/90°/0°/20^{\circ}/0^{\circ}/-20^{\circ}/0^{\circ}/40^{\circ}/0°/-40^{\circ}/0^{\circ}/60^{\circ}/0°/-60^{\circ}/0^{\circ}/80^{\circ}/0^{\circ}/-80^{\circ}/0°/90^{\circ}]$	E_{11}=158.5 E_{22}=78.95 E_{33}=23.15	G_{12}=19.82 G_{13}=4.74 G_{23}=5.529	μ_{12}=0.176 μ_{13}=0.304 μ_{23}=0.277
Model - 9		$[0^{\circ}/7.5°/-15°/22.5^{\circ}/-30^{\circ}/37.5°/-45^{\circ}/52.5^{\circ}/-60°/67.5°/-75^{\circ}/82.5^{\circ}/90°/0^{\circ}/-15°/-30°/-45^{\circ}/-60^{\circ}/-75^{\circ}/90^{\circ}]$	E_{11}=97.88 E_{22}=97.88 E_{33}=23.21	G_{12}=31.88 G_{13}=5.126 G_{23}=5.126	μ_{12}=0.237 μ_{13}=0.255 μ_{23}=0.255
Model - 10		$[0°/90°/0°/45°]_{5}$	E_{11}=137.8 E_{22}=80.2 E_{33}=23.04	G_{12}=18.05 G_{13}=5.401 G_{23}=4.838	μ_{12}=0.073 μ_{13}=0.309 μ_{23}=0.319

3. TESTING OF COMPOSITES

3.1 Tensile test

As indicated in Figure 1, tensile testing is carried out by cutting the composite specimen in line with ASTM Standard: D638. Measurements of this specimen. A total of ten models were built to test the tension resistance of ten models reinforced with various angles for various composite materials.

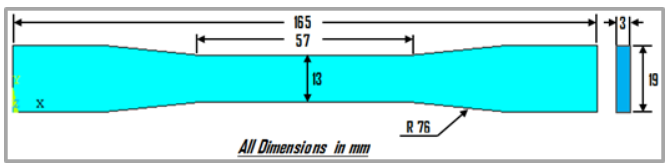

Figure 1. ASTM D638 standard tensile test model [28]

3.2 Compressive test

The test sample and dimension for the compression test are shown in Figure 2, using the compression apparatus of ASTM D3518/M [29]. Ten models were constructed to test the compressive resistance of ten models reinforced with different angles for different composite materials.

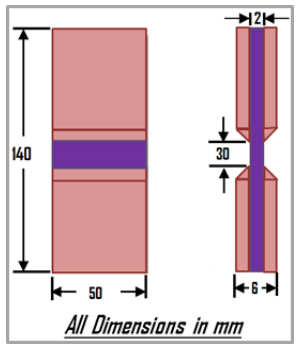

Figure 2. Schematic arrangement of 3-point bend test [29]

4. RESULTS AND DISCUSSION

4.1 Codes

Figure 3 illustrations the order of the ten codes that have been selected for comparison in terms of strains, stresses, deformation, and displacements, which result from the exposure of these models consisting of composite and reinforced materials at different angles according to the codes in the figure to a tension load.

Figure 3. The selected codes

4.2 Tensile test

Ten composite material models that were created using the three-dimensional ANSYS software each have a unique code that sets it apart from the others. To examine how the ten models behaved when under the influence of a drag load, these models were evaluated with a drag load of 1600 N. As well as comparing among the ten selected models to find the deformations, displacements, strains, and stresses that they exhibit. Then choose the best model out of the ten to carry the two components of the code that can withstand this kind of load and function securely in industrial, construction, space, maritime, military, and any other domains. The maximum deformations of the ten models are depicted in Figure 4 together with their shapes and values; the fifth model had the highest value of the deformation (29.9026 mm), while the first model had the lowest value of the deformation (1.94228 mm).

The von Mises stress value of a material can be used to determine whether it will yield or fracture. Ductile materials are used the majority of the time. A material will yield if the von Mises stress is equal to or greater than the yield limit of the same material under simple tension. According to the von Mises yield criterion. In light of this, Figure 5 shows that the best model, with a von Mises stress value of (2302.94 MPa), was the fifth model. According to the von Mises stress theory, this model is more resistant to collapsing than the other nine models. The worst of the ten models, the third one, collapses the fastest while having the largest von Mises stress value (4864.89 MPa).

The horizontal path (x-x) used to compare the deformations and normal stresses that take place in the models when they are subjected to the identical tensile load is shown in Figure 6.

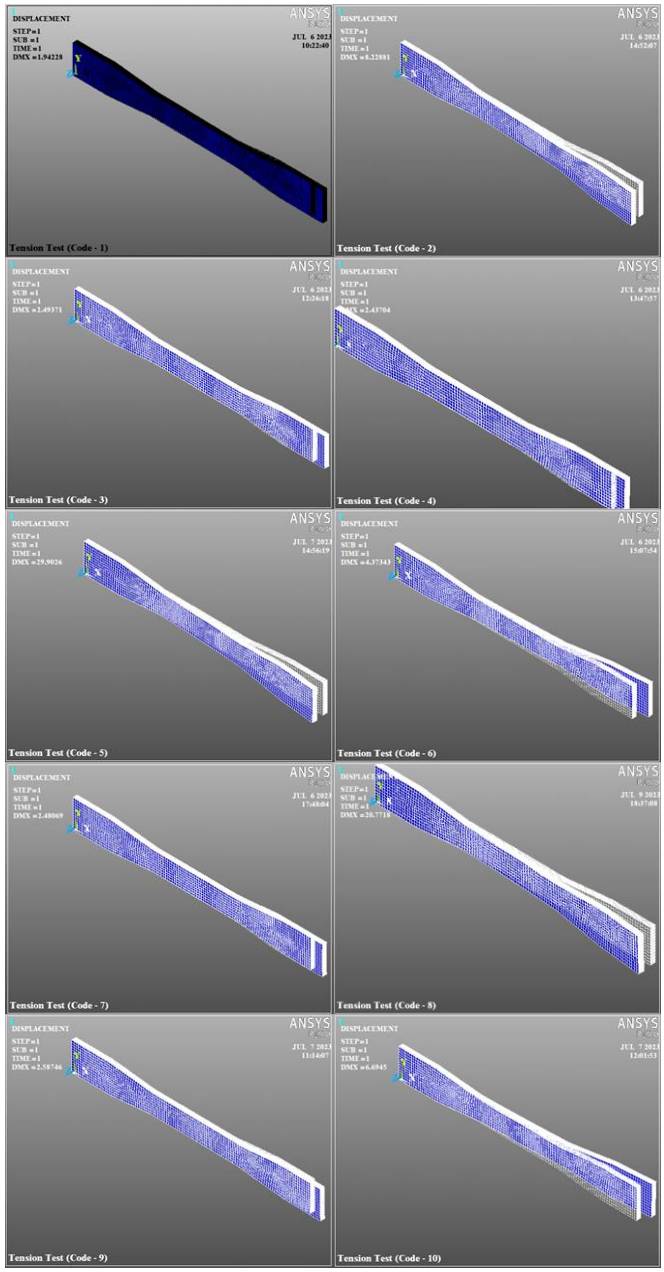

Figure 4. Deformation in all models

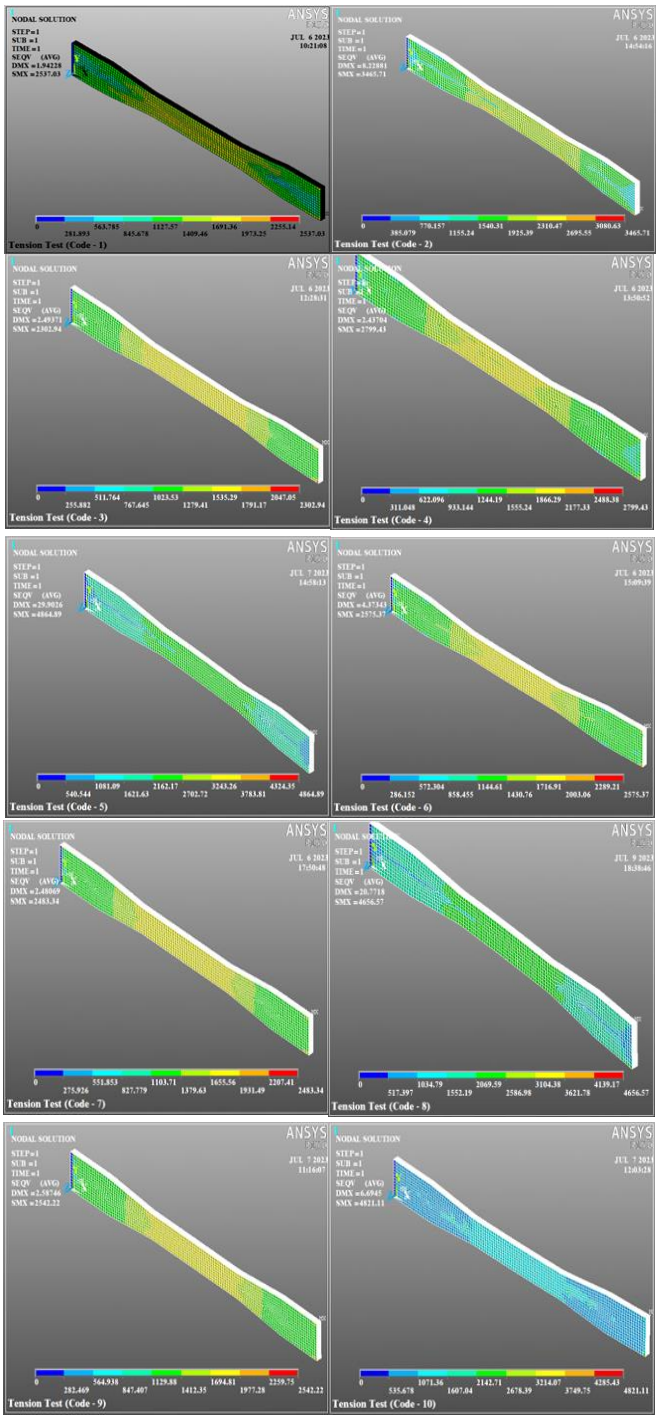

Figure 5. Comparison among von Mises stress of the tensile test in all codes

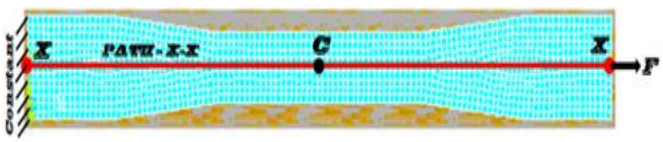

Figure 6. The chosen horizontal path for the tensile test

Figure 7 compares the deformations that the ten models underwent during the tensile test of the composite material on the path (x-x). The image appears to suggest that the first model had the lowest deformation values throughout the path (x-x), while the fifth model had the highest deformation values from the beginning of the deformation distribution on the models to the end.

In the tensile test of the composite material, the normal stress (σ_x), which affects all ten models, is compared in Figure 8 on the (x-x) path. The figure appears to show that the tenth model's curve on the same path had the lowest distortion values while the fifth model's curve had the greatest distortion values.

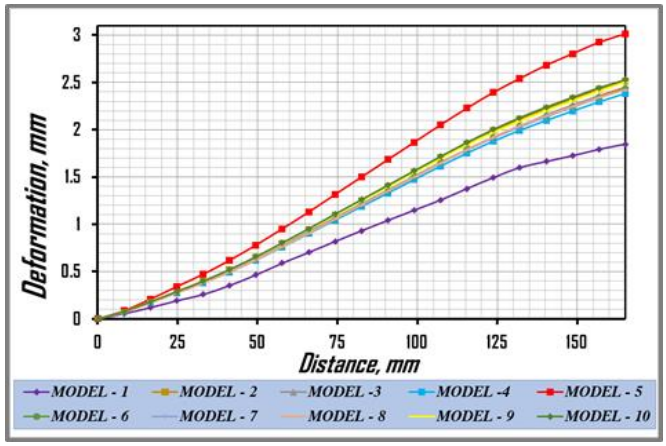

Figure 7. The comparison of tensile test deformation among all models

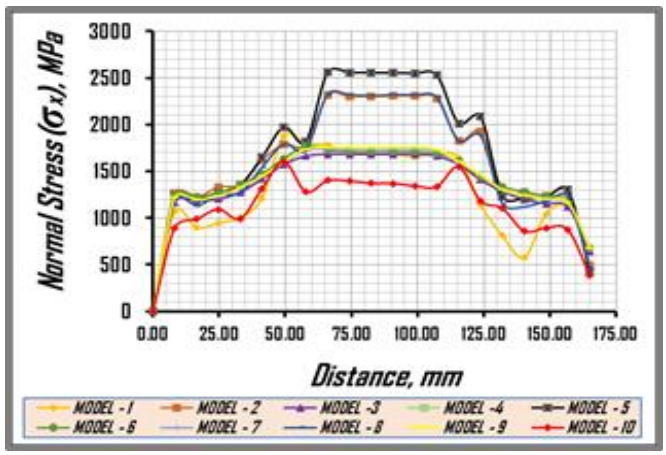

Figure 8. The comparison of tensile test normal stresses (σ_x) among all models

In Figures 9-22, the displacements, stresses, and strains of the ten models after loading with an applied load of 1600 N are shown together with the results from the ANSYS program at point (C) in the center of the model, whose value is (82.5 mm). The highest and lowest values were as follows:

Maximum value:	**Minimum value:**
$U_{x\text{-}M5}$=1.5002 mm;	$U_{x\text{-}M1}$=0.93149 mm;
$U_{y\text{-}M5}$=0.065053 mm;	$U_{y\text{-}M8}$= 0.018765 mm;
Usum-M5=6.007 mm;	$U_{sum\text{-}M1}$=0.93286 mm;
$\sigma_{x\text{-}M5}$=2557.2 MPa;	$\sigma_{x\text{-}M10}$= 1371.3 MPa;
$\sigma_{y\text{-}M10}$= 492.2 MPa;	$\sigma_{y\text{-}M3}$= 0.048186 MPa;
$\tau_{xy\text{-}M10}$= 219.13 MPa;	$\tau_{xy\text{-}M3}$=1.835 MPa;
$\sigma_{1\text{-}M5}$=2574.3 MPa;	$\sigma_{1\text{-}M10}$= 1422.9 MPa;
$\sigma_{int.\text{-}M5}$=2627.5 MPa;	$\sigma_{int.\text{-}M10}$= 1422.9 MPa;
$\sigma_{von\text{-}M5}$=2601.4 MPa;	$\sigma_{von\text{-}M10}$= 1261.7 MPa;
$\varepsilon_{x\text{-}M10}$= 0.019284;	$\varepsilon_{x\text{-}M1}$= 0.013432;
$\varepsilon_{y\text{-}M3}$=0.0052737;	$\varepsilon_{y\text{-}M1}$= 0.0033;
$\varepsilon_{xy\text{-}M1}$=0.013771;	$\varepsilon_{xy\text{-}M3}$= 0.0000503;
$\varepsilon_{int\text{-}M10}$= 0.02467;	$\varepsilon_{int\text{-}M8}$=0.018848;
$\varepsilon_{von\text{-}M10}$=0.022766.	$\varepsilon_{von\text{-}M8}$=0.01694.

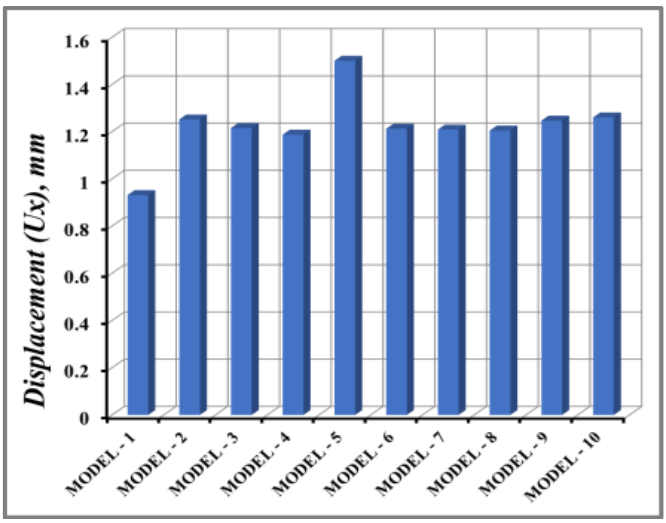

Figure 9. The comparison of tensile test displacement (U_x) in direction x-axis among all models

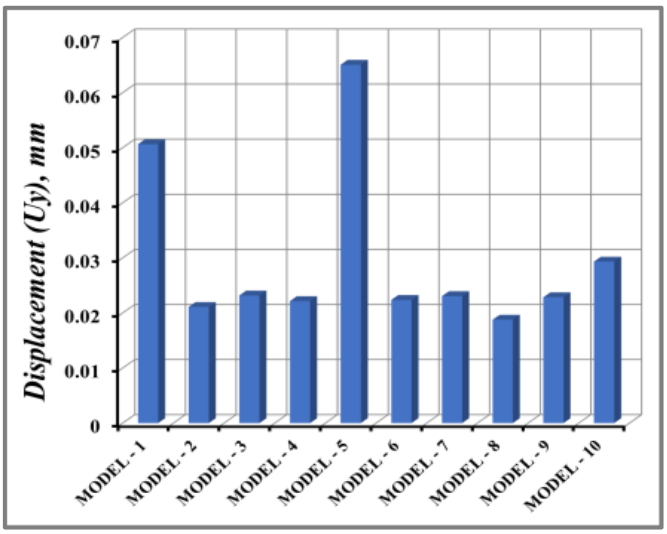

Figure 10. The comparison of tensile test displacement (U_y) in direction y-axis among all models

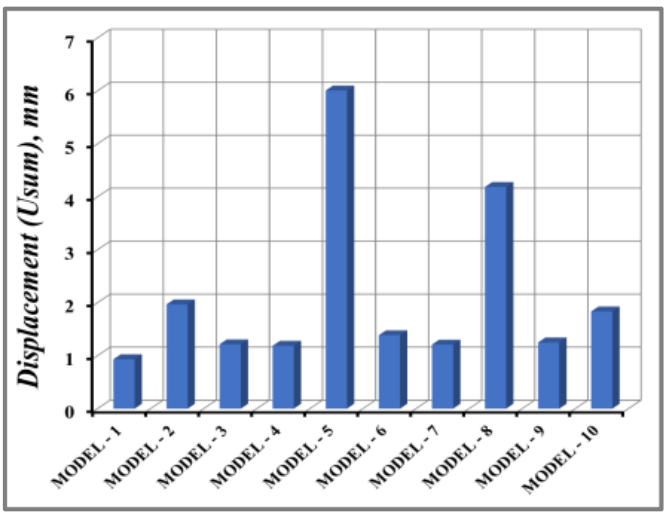

Figure 11. The comparison of tensile test displacement (U_{sum}) in direction x-axis among all models

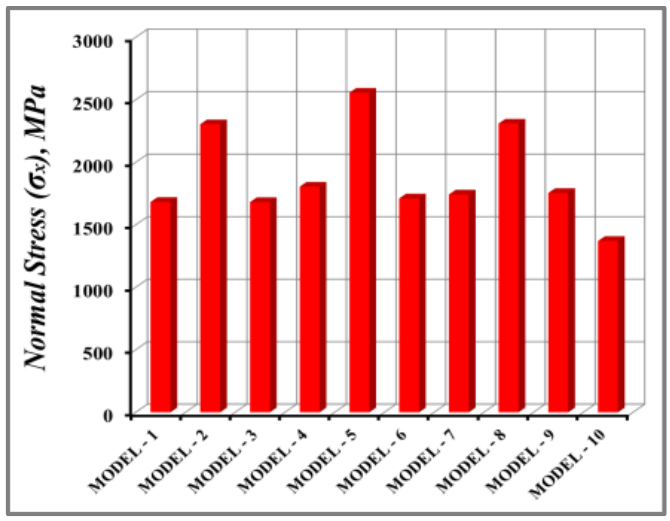

Figure 12. The comparison of tensile test normal stress (σ_x) among all models

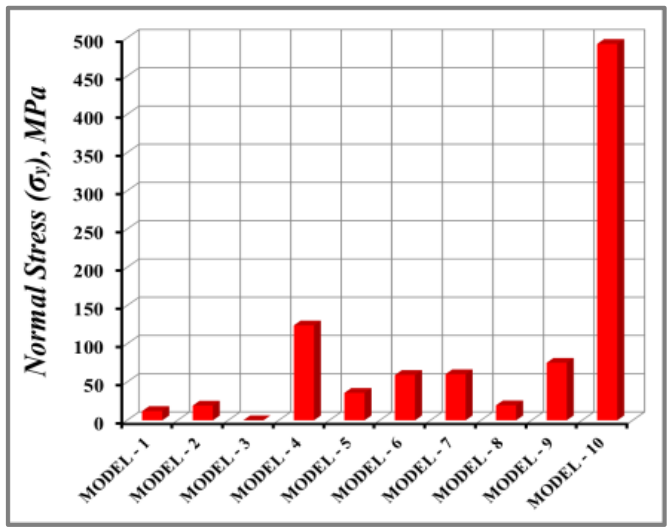

Figure 13. Normal stress (σ_y) in of the tensile test

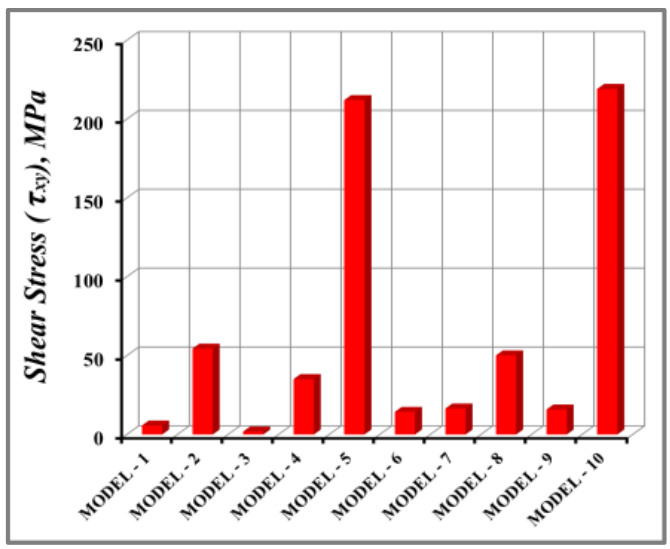

Figure 14. The comparison of tensile test shear stress (τ_{xy}) among all models

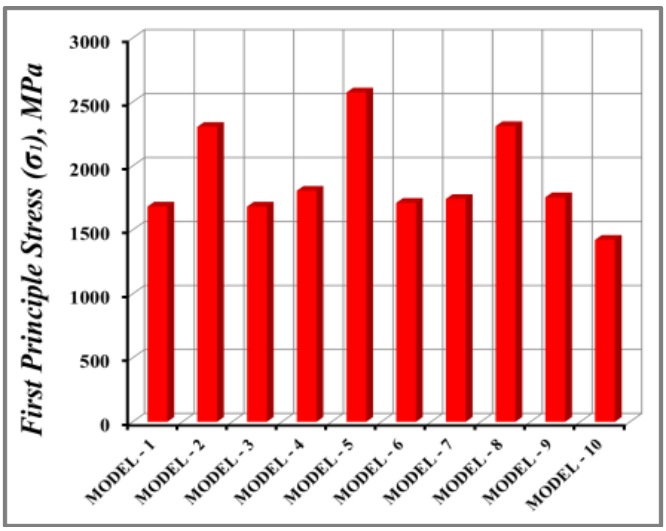

Figure 15. The comparison of tensile test principle stress (σ_1) among all models

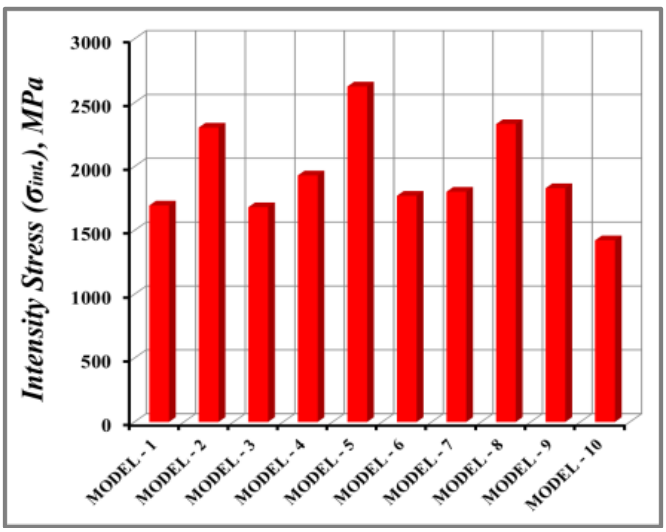

Figure 16. First The comparison of tensile test intensity stress ($\sigma_{int.}$) among all models

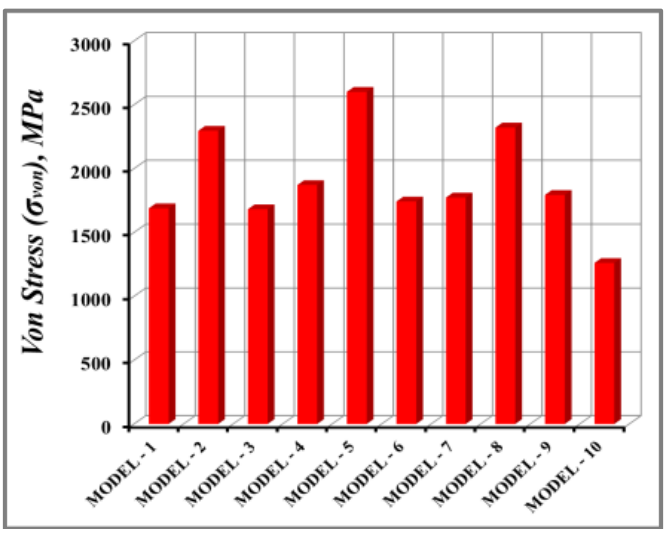

Figure 17. The comparison of tensile test von Mises stresses (σ_{von}) among all models

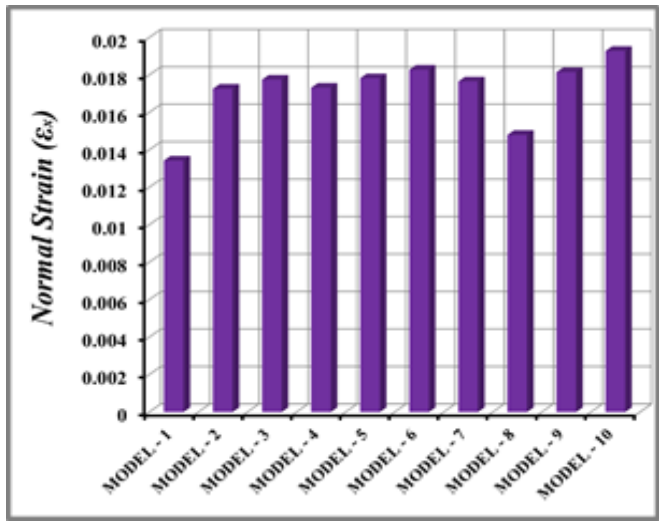

Figure 18. The comparison of tensile test normal strain (ε_x) among all models

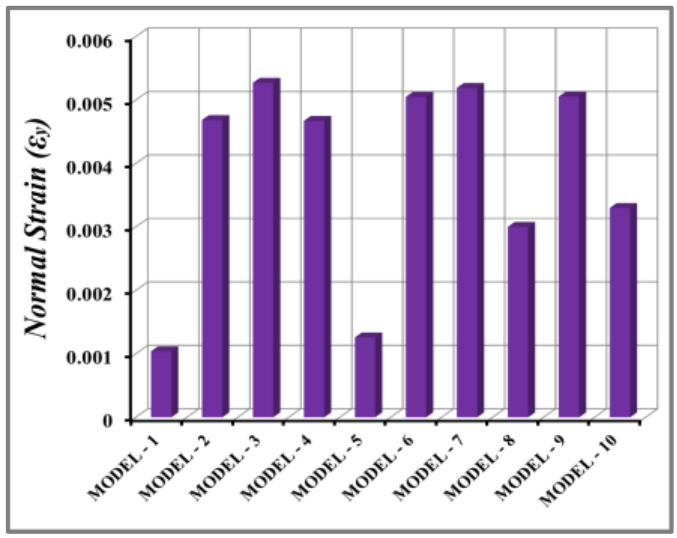

Figure 19. Normal strain (ε_y) in of the tensile test

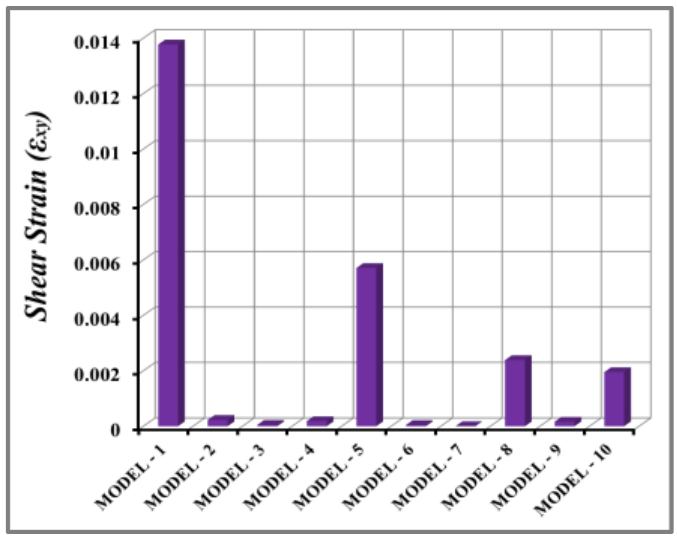

Figure 20. The comparison of tensile test shear strain (ε_{xy}), among all models

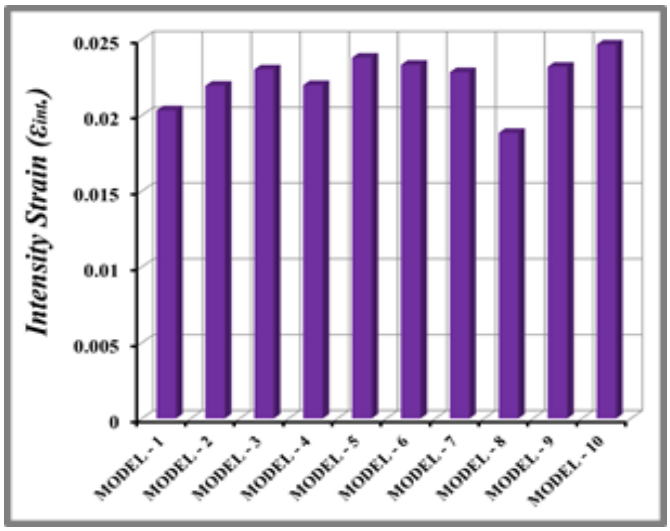

Figure 21. The comparison of tensile test intensity strain ($\varepsilon_{int.}$), among all models

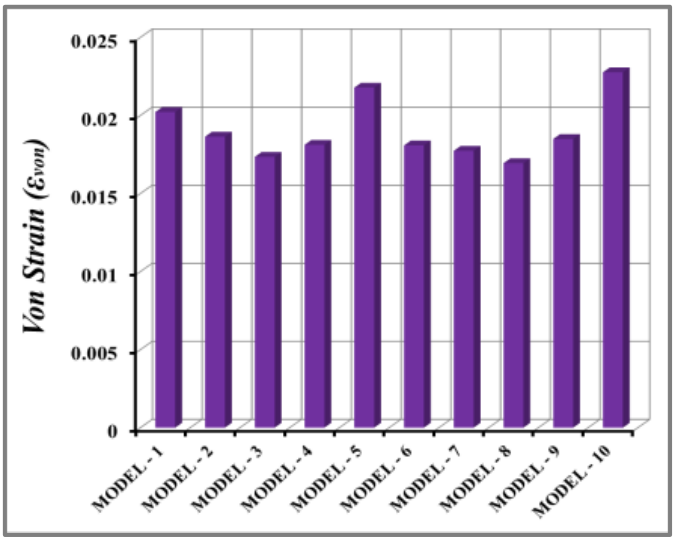

Figure 22. The comparison of tensile test von Mises strain (ε_{von}), among all models

4.3 Compressive test

Each of the ten composite material models produced by the three-dimensional ANSYS program has a special code that distinguishes it from the others. The ten models were tested with a compressive load of 1600 N to examine how they responded to the influence of a compressive force. Additionally, the deformations, displacements, strains, and stresses displayed by the ten chosen models were compared. Then decide which of the ten designs can safely hold the two code components and withstand this kind of load in industrial, construction, space, maritime, military, and other areas. Figure 23 shows the forms and values of the ten models' maximum deformations. The fifth model had the greatest number of deformations (0.238476 mm), while the first model had the smallest amount of deformation (0.154287 mm).

It is possible to foretell whether a material will give or fracture using its von Mises stress value. The most common material used is ductile. The von Mises yield criterion states that a material will yield if the von Mises stress is equal to or greater than the yield limit of the same material under simple compression. Figure 24 shows that, in accordance with the von Mises stress theory, the fifth model, with a von Mises stress value of (2302.94 MPa), is the best option since it is less susceptible to collapsing than the other nine models. The worst of the ten models, the third one, collapses the fastest while having the largest von Mises stress value (4864.89 MPa).

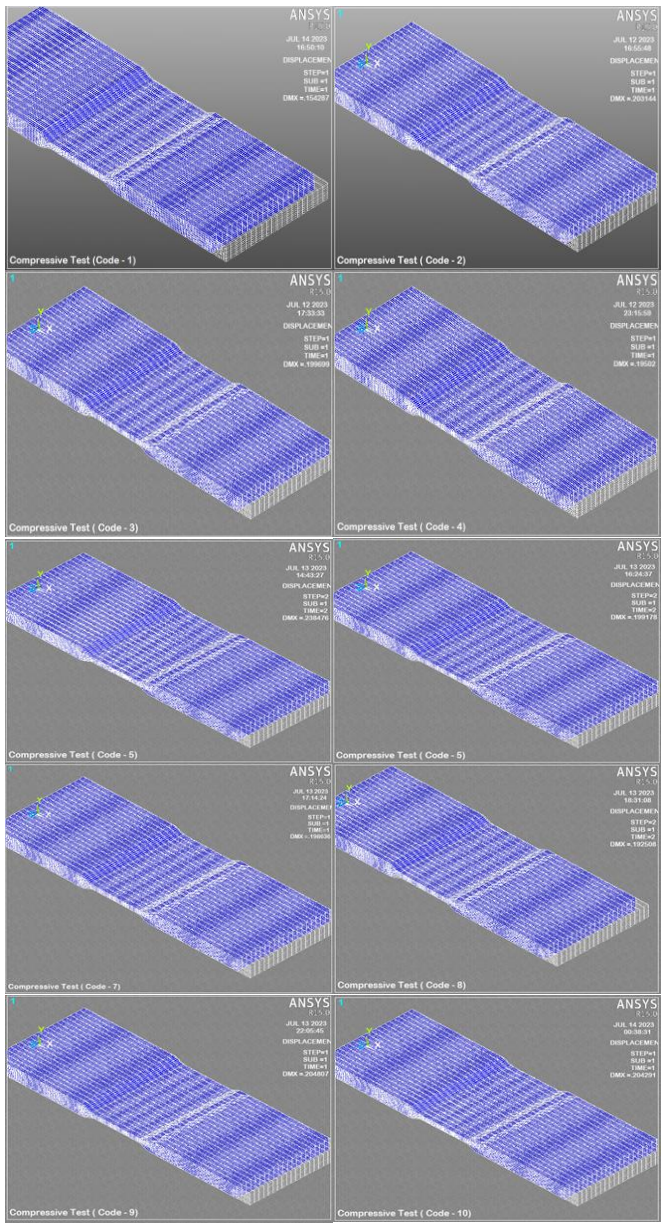

Figure 23. Deformation in all models

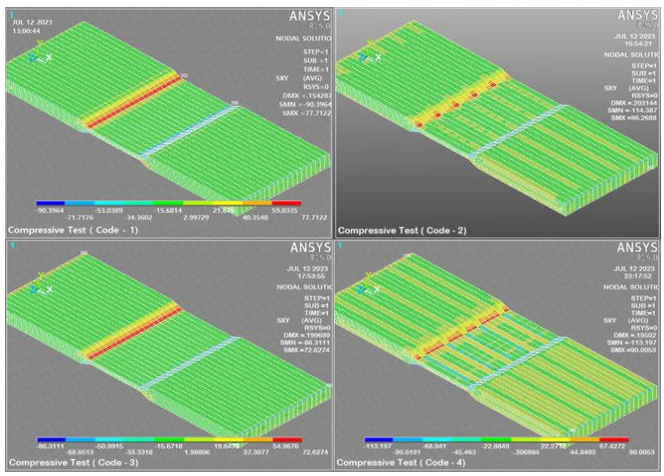

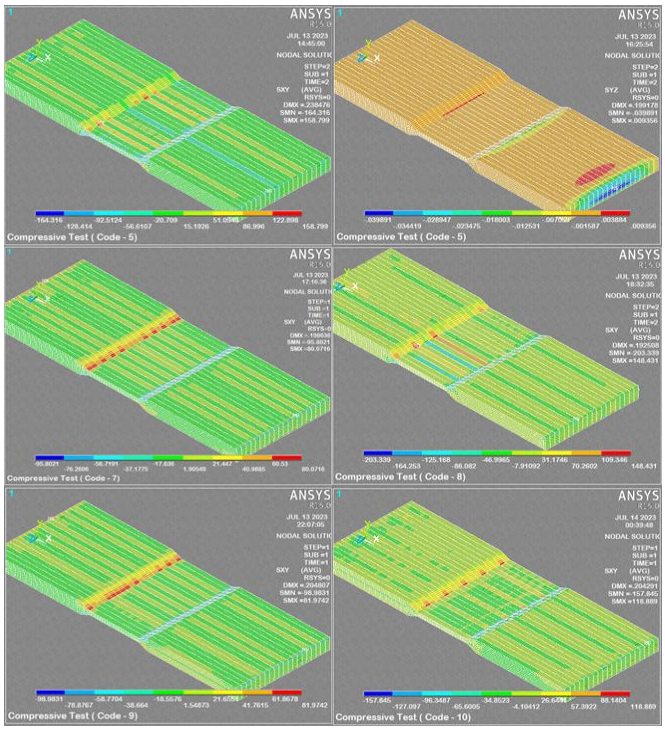

Figure 24. Comparison among shear stress of the compressive test in all codes

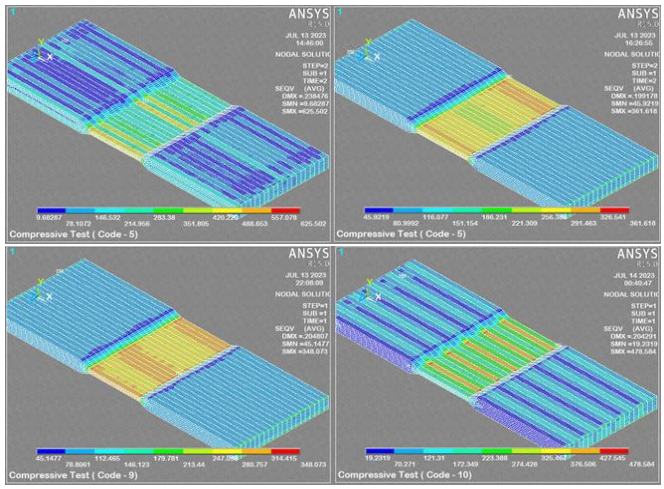

Figure 25. Comparison among von Mises stress of the compressive test in all codes

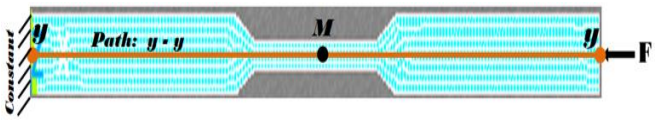

Figure 26. Illustrations of the chosen horizontal path for the compressive test

The von Mises stress value of a material can be used to forecast whether it will yield or fracture. The most often used materials are ductile. The von Mises yield criterion states that if the von Mises stress is equal to or greater than the material's yield limit under simple compression, the material will yield. Figure 25 shows that, in accordance with the von Mises stress theory, the fifth model, with a von Mises stress value of (625.252 MPa), is the best option since it is less susceptible to collapsing than the other nine models. The worst of the ten models, the third one, collapses the fastest while having the largest von Mises stress value (325.252 MPa).

In order to compare the deformations, normal stresses, shear stresses, intensity stresses, and von Mises stresses that take place in the models when they are subjected to the identical compressive load, the horizontal path (y-y) that was selected, Figure 26.

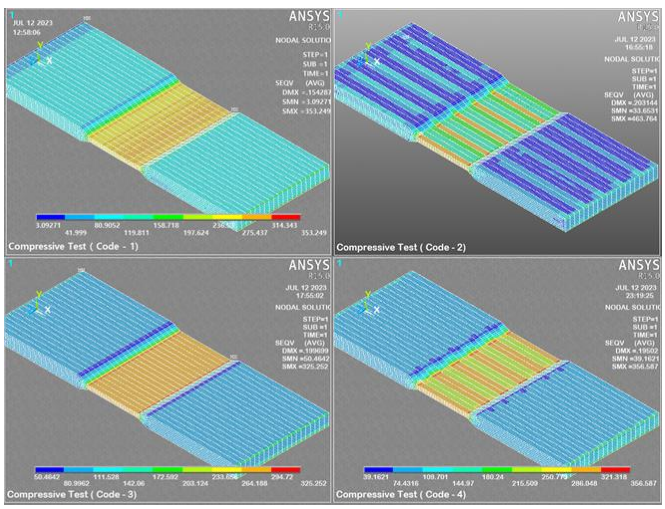

Figure 27 compares the deformations that the ten models underwent during the compressive test of the composite material on the path (y-y). According to the figure, the first model had the lowest deformation values along the same path from the beginning of the deformation distribution on the models to its conclusion (y-y), while the fifth model had the highest values along the same path.

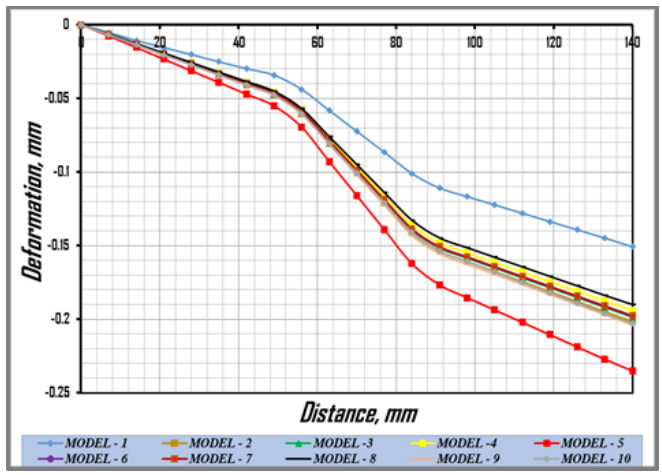

Figure 27. The comparison of compressive test deformation among all models

Figure 28 compares the normal stress (σ_x) on the (y-y) path in the tensile test of the composite material, which has an impact on all ten models. The figure seems to indicate that, on the same path, the tenth model's curve had the least distortion values while the fifth model's curve had the most distortion values.

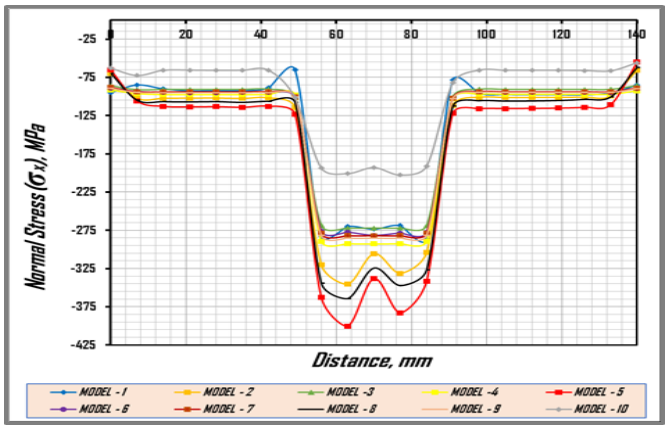

Figure 28. The comparison of compressive test normal stresses (σ_x) among all models

The theory of maximum shear stress provides a framework for examining the stress-related failure of ductile materials. When creating safe parts, it is crucial to adhere to this standard. The theory is concerned with determining the highest shear stress value at which a material will eventually deform. The shear stress (τ_{xy}), which affects all ten models in the compressive test of the composite material, is contrasted on the (y-y) path in Figure 29. According to the figure, the fifth model's curve had the highest distortion values and the ninth model's curve had the lowest distortion values for the same path.

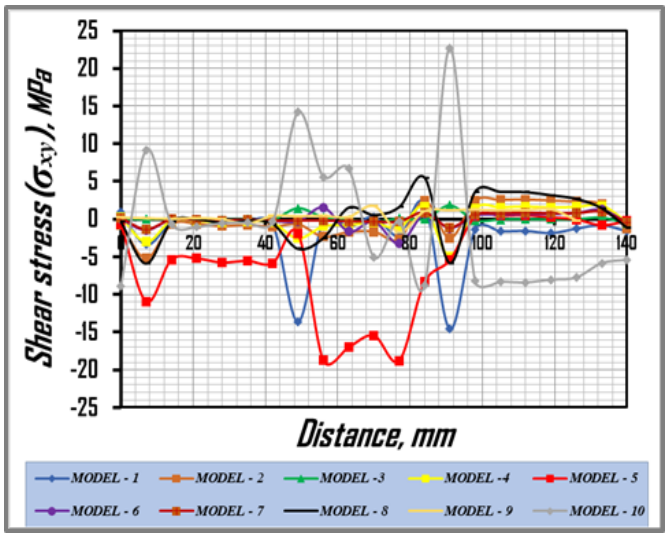

Figure 29. The comparison of compressive test shear stresses (τ_{xy}) among all models

In Figure 30, the (y-y) path contrasts the intensity stress ($\sigma_{int.}$), which is present in all ten models during the compressive test of the composite material. The figure shows that over the identical path, the distortion values for the curves of the fifth and tenth models were highest and lowest respectively.

The von Mises stress (σ_{von}), which is present in all ten models throughout the compressive test of the composite material, is contrasted in Figure 31 by the (y-y) route. The figure demonstrates that for the fifth and tenth models' curves, the distortion values were largest and lowest, respectively, across the same path.

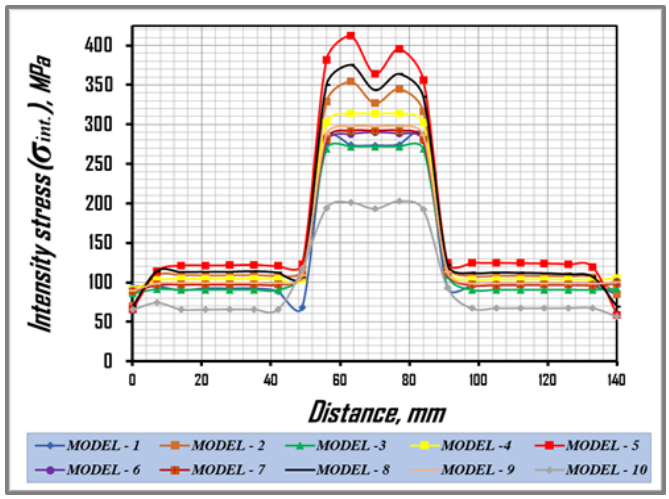

Figure 30. The comparison of compressive test intensity stresses ($\sigma_{int.}$) among all models

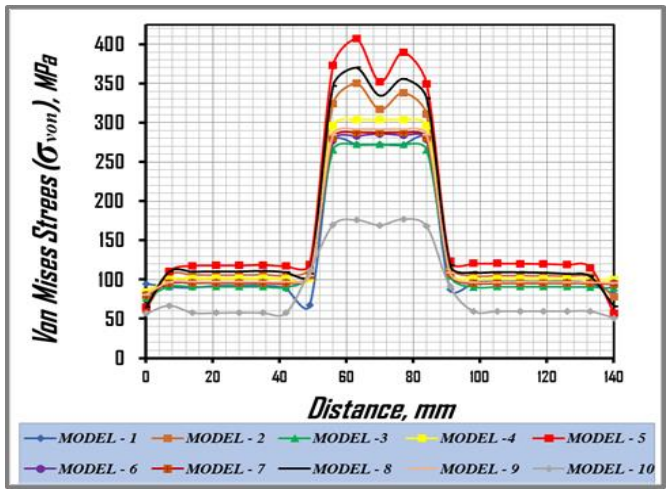

Figure 31. The comparison of compressive test von Mises stresses (σ_{von}) among all models

In Figures 32 to 45, along with the results of the ANSYS software at the model's center, point (M), whose value is (70 mm), are the displacements, stresses, and strains of the ten models after being loaded with a 1600 N applied load. These were the highest and lowest values, respectively:

Maximum value:

$U_{x\text{-}M5}$=0.10074 mm;
$U_{y\text{-}M1}$=0.00883 mm;
$U_{sum\text{-}M10}$=0.19971 mm;
$\sigma_{x\text{-}M5}$=247.56 MPa;
$\sigma_{y\text{-}M10}$= 70.575 MPa;
$\tau_{xy\text{-}M5}$= 15.435 MPa;
$\sigma_{1\text{-}M5}$=25.34 MPa;
$\sigma_{int.\text{-}M5}$=364.1 MPa;
$\sigma_{von\text{-}M5}$=352.11 MPa;
$\varepsilon_{x\text{-}M5}$= 0.003218;
$\varepsilon_{y\text{-}M3}$=0.00508528;
$\varepsilon_{xy\text{-}M5}$=0.000945;
$\varepsilon_{int\text{-}M5}$= 0.0004389;
$\varepsilon_{von\text{-}5}$=0.004045.

Minimum value:

$U_{x\text{-}M5}$=0.0116 mm;
$U_{y\text{-}M2}$= 0.000754 mm;
$U_{sum\text{-}M1}$=0.072906 mm;
$\sigma_{x\text{-}M10}$= 192.98 MPa;
$\sigma_{y\text{-}M3}$= 0.00897 MPa;
$\tau_{xy\text{-}M1}$=0.304 MPa;
$\sigma_{1\text{-}M1\&10}$= 0.000 MPa;
$\sigma_{int.\text{-}M10}$= 193.19 MPa;
$\sigma_{von\text{-}M10}$= 169.35 MPa;
$\varepsilon_{x\text{-}M1}$= 0.0020367;
$\varepsilon_{y\text{-}M1}$= 0.0033;
$\varepsilon_{xy\text{-}M1}$= 0.0000102;
$\varepsilon_{int\text{-}M7}$=0.00001017;
$\varepsilon_{von\text{-}M1}$=0.00244.

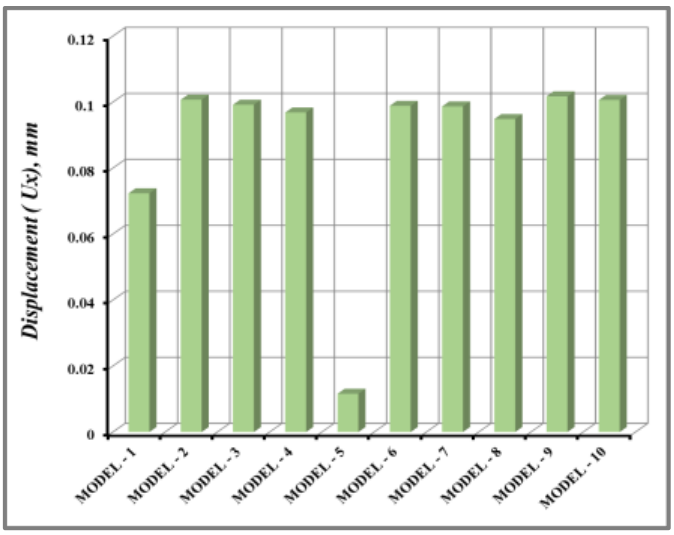

Figure 32. The comparison of compressive test displacement (U_x) in direction x-axis among all models

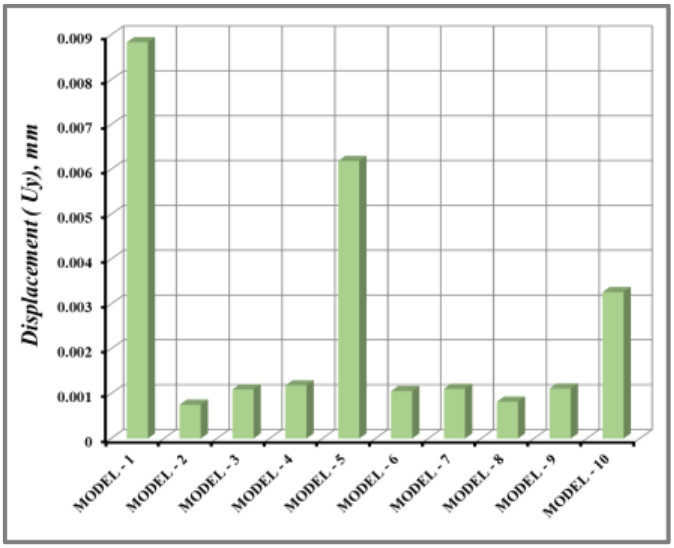

Figure 33. The comparison of compressive test displacement (U_y) in direction y-axis among all models

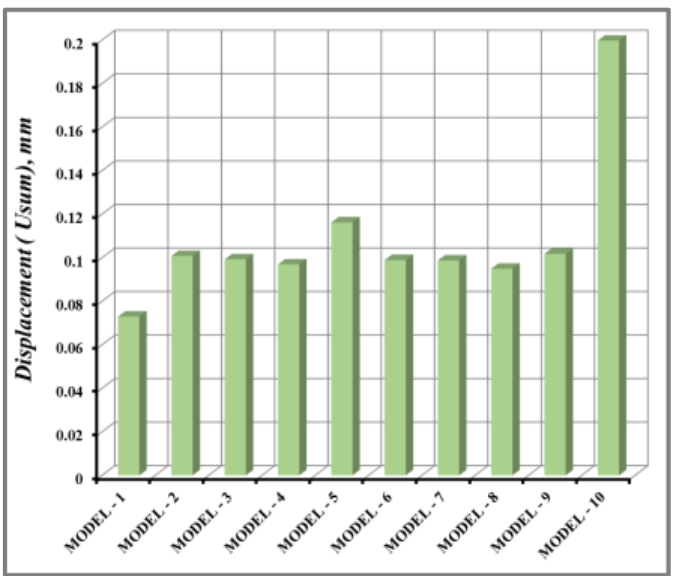

Figure 34. The comparison of compressive test displacement (U_{sum}) in direction x-axis among all models

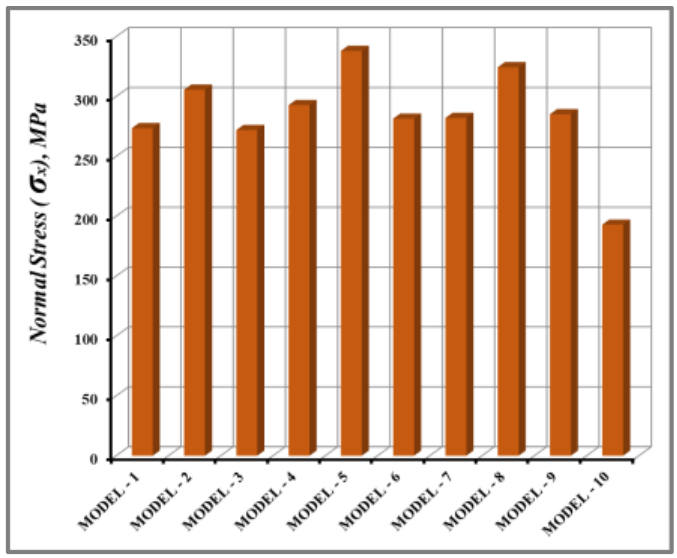

Figure 35. The comparison of compressive test normal stress (σ_x) among all models

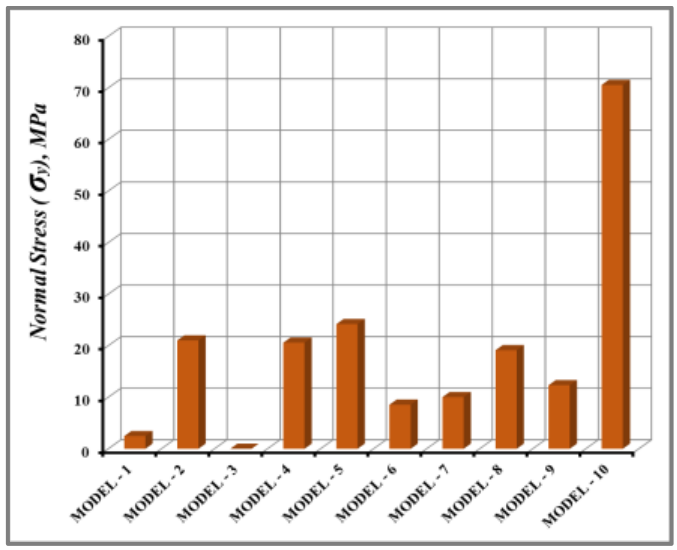

Figure 36. Normal stress (σ_y) in of the compressive test

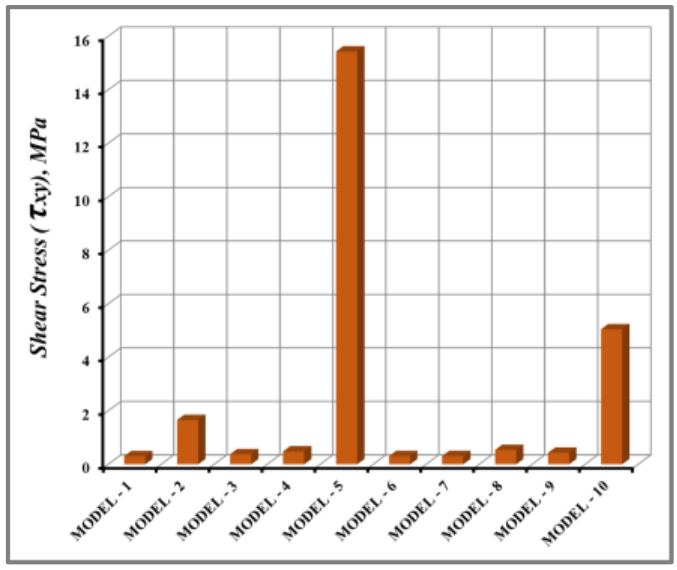

Figure 37. The comparison of compressive test shear stress (τ_{xy}) among all models

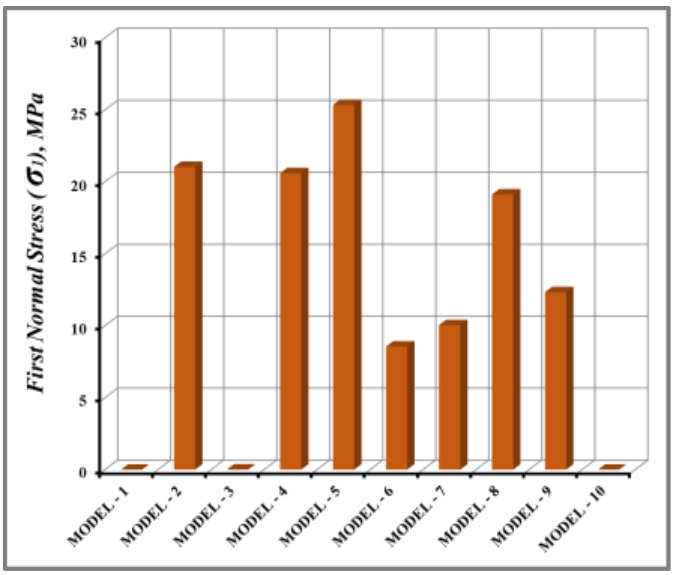

Figure 38. The comparison of compressive test principle stress (σ_1) among all models

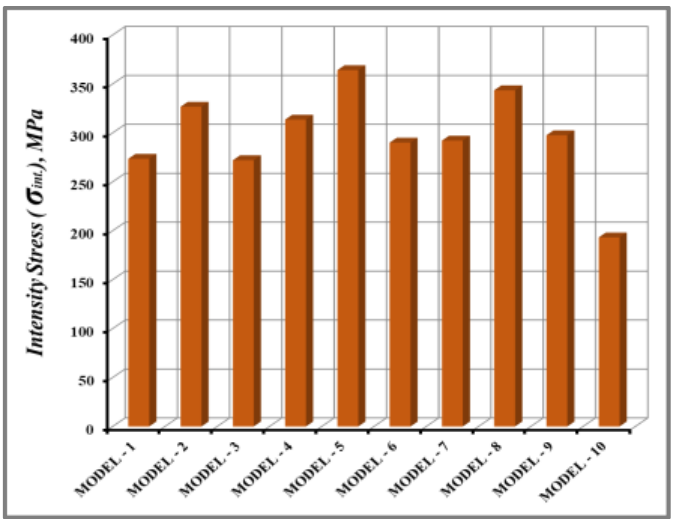

Figure 39. First comparison of compressive test intensity stress ($\sigma_{int.}$) among all models

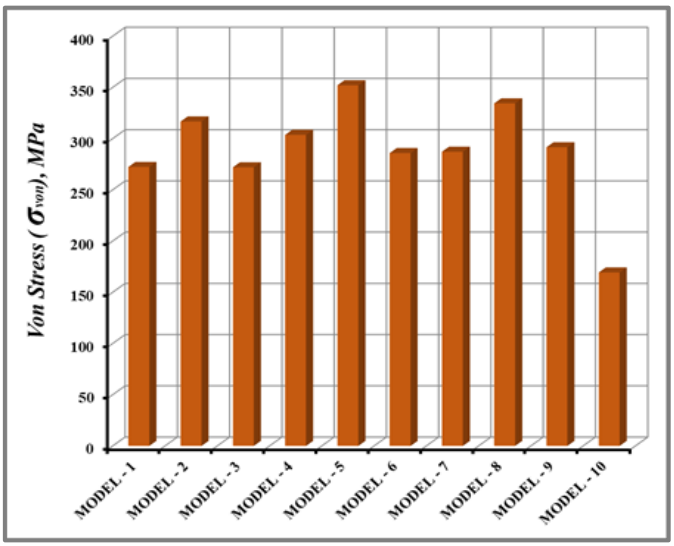

Figure 40. The comparison of compressive test von Mises stresses (σ_{von}) among all models

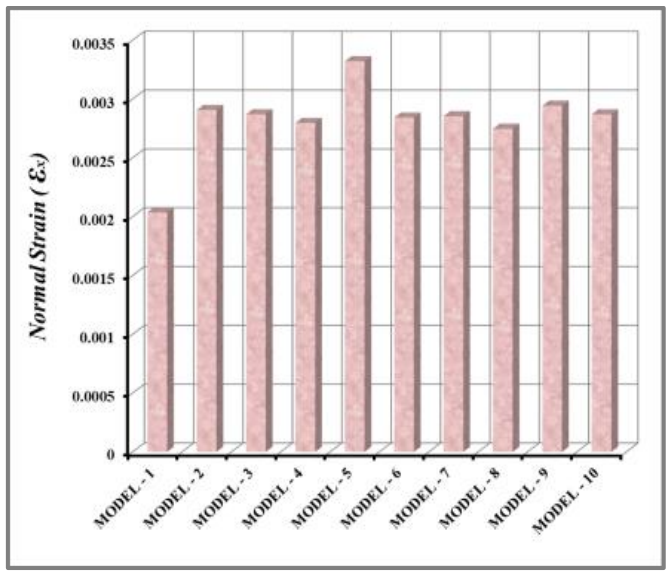

Figure 41. The comparison of compressive test normal strain (ε_x) among all models

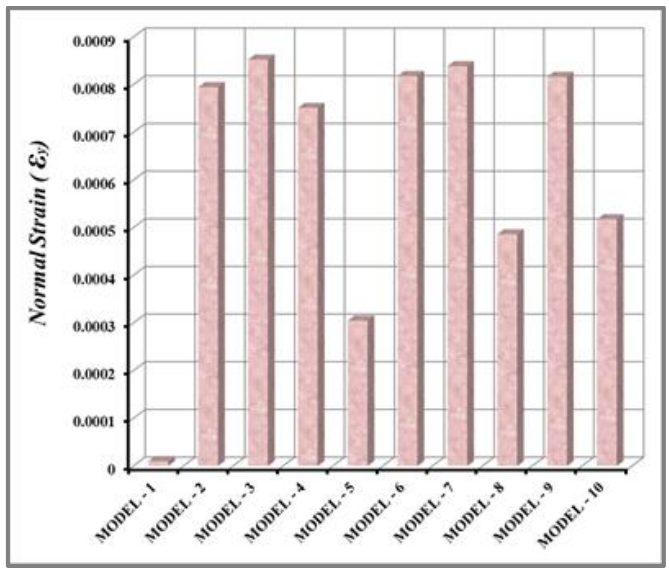

Figure 42. Normal strain (ε_y) in of the compressive test

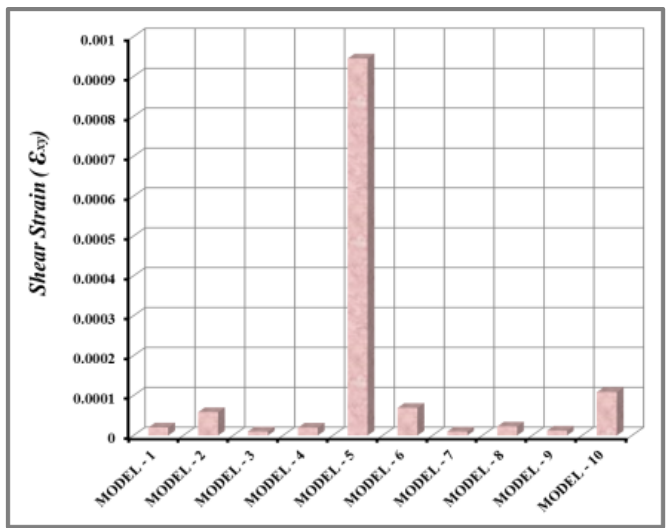

Figure 43. The comparison of compressive test shear strain (ε_{xy}), among all models

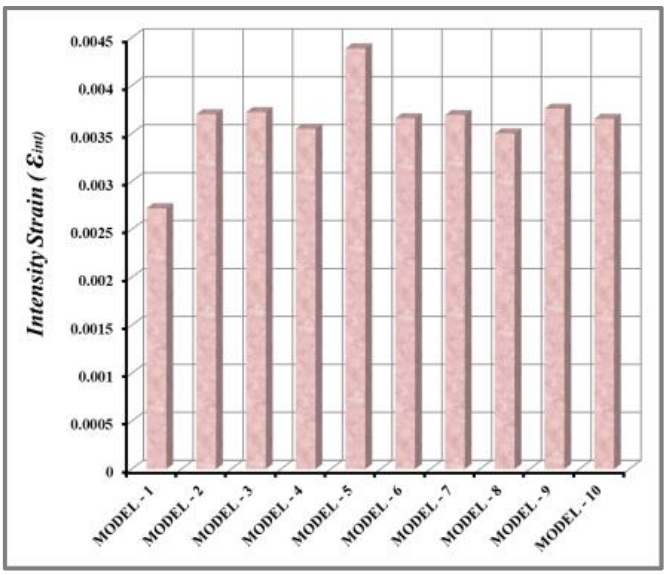

Figure 44. The comparison of compressive test intensity strain ($\varepsilon_{int.}$), among all models

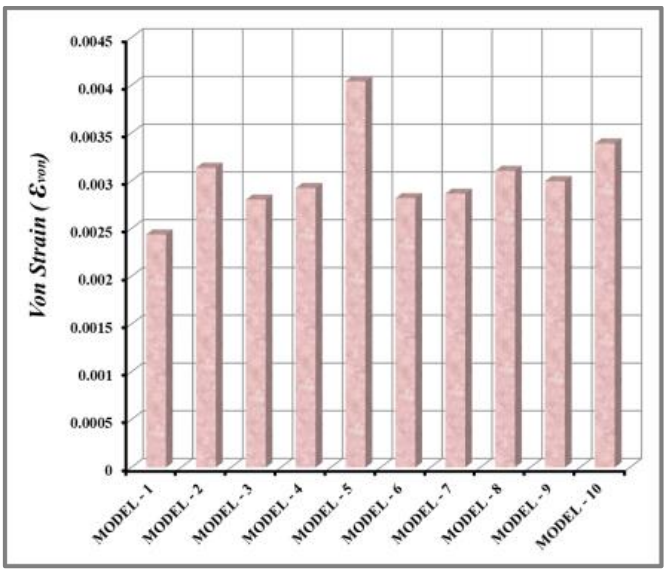

Figure 45. The comparison of compressive test von Mises strain (ε_{von}), among all models

5. CONCLUSIONS

To evaluate the mechanical characteristics of CFRP composite chips, such as tensile and compressive properties, bending, and impact resistance, the ANSYS program was used to construct ten models, each built of composite material and furnished with various angles from the other using different codes. The results showed the following:

1. By using the von Mises stress theory of failure, the results of the tensile testing of the models were demonstrated. The tenth model is the most failure-resistant of all the models. Compared to the resistance to the fifth model's breakdown, the resistance to collapse is lower (51.5%).

2. The results of the compressive testing of the models were shown using the von Mises stress theory of failure. The third model is the one that is least likely to fail. The resistance to collapse is less (48%) than the resistance to the disintegration of the fifth model.

3. The path (y-y) is affected by shear stress. Observe that, as a result of the compression test, the tenth model has the highest shear stress and its value is 22.734 MPa, while the sixth model has the lowest shear stress and its value is 1.5686 MPa.

4. The third model is the best model for resistance to stresses, strains, and deformations under the effect of the tensile test and the compression test, it is inferred from the study of the results of ten models tests.

6. RECOMMENDATIONS AND FUTURE WORK

The need for materials that can satisfy the complicated requirements of contemporary applications while supporting sustainability goals is a problem shared by industries worldwide in an era of rapid technical innovation and growing environmental concerns. Conventional materials frequently fall short of offering the ideal combination of qualities needed for cutting-edge applications, including sustainability, design flexibility, strength and durability, and weight reduction. Since composite materials are employed in this article, the following are the most crucial suggestions for further research in this area to create a balance of the aforementioned properties:

1. Undertaking comprehensive scientific investigations concerning composite materials technology, encompassing Nano composites, bio-based composites, and smart composites.

2. Undertaking investigations and studies to examine the possible effects of advanced composites in several industries,

3. Investigating, studying about, and debating the potential and difficulties in implementing and extending the use of composite materials technology,

4. Investigating and studying alternative composite materials, varying the angles of reinforcement, and performing mechanical tests for fatigue resistance, bending strength, impact resistance, tensile strength, corrosion resistance, and other critical mechanical tests in a range of technological, industrial, and military applications.

REFERENCES

[1] Karash, E.T., Sultan, J.N., Najem, M.K. (2021). The difference in the wall thickness of the helicopter structure are made of composite materials with another made of steel. Mathematical Modelling of Engineering Problems, 9(2): 313-324. https://doi.org/10.18280/mmep.090204

[2] Najem, M.K., Karash, E.T., Sultan, J.N. (2022). The amount of excess weight from the design of an armored vehicle body by using composite materials instead of steel. Revue des Composites et des Matériaux Avancés-Journal of Composite and Advanced Materials, 32(1): 1-10. https://doi.org/10.18280/rcma.320101

[3] Karash, E.T. (2011). Modelling of unilateral contact of metal and fiberglass shells. Applied Mechanics and Materials Journal, 87: 206-208. https://doi.org/10.4028/www.scientific.net/AMM.87.20

[4] Karash, E.T., Alsttar Sediqer, T.A., Elias Kassim, M.T. (2021). A comparison between a solid block made of concrete and others made of different composite materials. Revue des Composites et des Matériaux Avancés, 31(6): 341-347. https://doi.org/10.18280/RCMA.310605

[5] Barschke, M., Pardo, D.A.U., Jensen, J.L., Zapata, C.E.L. (2009). Finite element modeling of composite materials using kinematic constraints. Ingeniería y Ciencia, 5(10): 133-153.
[6] Rimal, A., Natarajan, V.D. (2024). Comparative analysis of aerodynamic and structural performance of aircraft wings using boron aluminum metal matrix composites and aluminum alloys: A CFD and FSI approach. Precision Mechanics & Digital Fabrication, 1(2): 75-90. https://doi.org/10.56578/pmdf010203
[7] Elias Kassim, M.T., Karash, E.T., Sultan, J.N. (2023). A mathematical model for non-linear structural analysis reinforced beams of composite materials. Mathematical Modelling of Engineering Problems, 10(1): 311-333. https://doi.org/10.18280/mmep.100137
[8] Schwartz, M.M. (1997). Composite materials: Properties, nondestructive testing and repair. V.1, Prentice- Hall Inc., New Jersey, USA.
[9] Baker, A.A., Callus, P.J., Georgiadis, S., Falzon, P.J., Dutton, S.E., Leong, K.H. (2002). An affordable methodology for replacing metallic aircraft panels with advanced composites. Composites Part A: Applied Science and Manufacturing, 33(5): 687-696. https://doi.org/10.1016/S1359-835X(02)00013-1
[10] Sela, N., Ishai, O. (1989). Interlaminar fracture toughness and toughening of laminated composite materials: A review. Composites, 20(5): 423-435. https://doi.org/10.1016/0010-4361(89)90211-5
[11] Mouritz, A.P., Leong, K.H., Herszberg, I. (1997). A review of the effect of stitching on the in-plane mechanical properties of fiber-reinforced polymer composites. Composites Part A: Applied Science and Manufacturing, 28(12): 979-991. https://doi.org/10.1016/S1359-835X(97)00057-2.
[12] Aljumaili, M.W., Beddu, S., Itam, Z., Their, J.M. (2024). Mechanical characteristics and durability of metakaolin-based self-compacting geopolymer concrete as a function of recycled aggregate and steel fiber contents. Journal of Composite & Advanced Materials/Revue des Composites et des Matériaux Avancés, 34(4): 465-480. https://doi.org/10.18280/rcma.340408
[13] Wang, H., Zhao, X., Deng, Y. (2023). Examining the influence of thermal stress on the seismic resilience of prefabricated box culverts. International Journal of Heat & Technology, 41(5): 1264-1272. https://doi.org/10.18280/ijht.410516
[14] Peng, Z. (2021). Performance prediction and mix ratio optimization for multielement green high performance fiber-reinforced cement matrix composite. Annales de Chimie - Science des Matériaux, 45(1): 59-67. https://doi.org/10.18280/acsm.450108
[15] Loganathan, M., Dinesh, S., Vijayan, V., Ranjithkumar, M., Rajkumar, S. (2020). Experimental investigation of tensile strength of fiber reinforced polyester by using chicken feather fiber. Journal of New Materials for Electrochemical Systems, 23(1): 40-44. https://doi.org/10.14447/jnmes.v23i1.a08
[16] Karash, E.T., Ali, H.M., Elias Kassim, M.T. (2024). Designing cantilever models from various materials and comparing them when they are under constant load and have holes. Journal of Composite & Advanced Materials/Revue des Composites et des Matériaux Avancés, 34(3): 363-377. https://doi.org/10.18280/rcma.340312
[17] Dwivedi, S.P., Maurya, N.K., Maurya, M. (2019). Effect of uncarbonized eggshell weight percentage on mechanical properties of composite material developed by electromagnetic stir casting technique. Revue des Composites et des Matériaux Avancés, 29(2): 101-107. https://doi.org/10.18280/rcma.290205
[18] Banakar, P., Shivananda, H.K., Niranjan, H.B. (2012). Influence of fiber orientation and thickness on tensile properties of laminated polymer composites. International Journal of Pure and Applied Sciences and Technology, 9(1): 61-68.
[19] Liu, G., Zhang, L., Guo, L., Liao, F., Zheng, T., Zhong, S. (2019). Multi-scale progressive failure simulation of 3D woven composites under uniaxial tension. Composite Structures, 208: 233-243. http://doi.org/10.1016/j.compstruct.2018.09.081
[20] Jin, L., Niu, Z., Jin, B.C., Sun, B., Gu, B. (2012). Comparisons of static bending and fatigue damage between 3D angle-interlock and 3D orthogonal woven composites. Journal of Reinforced Plastics and Composites, 31(14): 935-945. http://doi.org/10.1177/0731684412450626
[21] Ma, Z., Zhang, P., Zhu, J. (2022). Influence of fabric structure on the tensile and flexural properties of three-dimensional angle-interlock woven composites. Journal of Industrial Textiles, 51(10): 1641-1657. http://doi.org/10.1177/1528083720906804
[22] Anuse, V.S., Shankar, K., Velmurugan, R., Ha, S.K. (2022). Compression-After-Impact analysis of carbon fiber reinforced composite laminate with different ply orientation sequences. International Journal of Impact Engineering, 167: 104277. https://doi.org/10.1016/j.ijimpeng.2022.104277
[23] Sulardjaka, S., Iskandar, N., Nugroho, S., Alamsyah, A., Prasetya, M.Y. (2022). The characterization of unidirectional and woven water hyacinth fiber reinforced with epoxy resin composites. Heliyon, 8(9): e10484. https://doi.org/10.1016/j.heliyon.2022.e10484
[24] Garbowski, T. (2022). Mechanics of corrugated and composite materials. Materials, 15(5): 1837. http://doi.org/10.3390/books978-3-0365-4313-0
[25] Mohamed, B., Khaoula, A., Leila, B. (2023). Effect of the fibers orientation of the different types of composite plates notched of U-shape repaired by composite patch. Materials Research, 26: e20220302. https://doi.org/10.1590/1980-5373-MR-2022-0302
[26] Korneeva, N.V., Kudinov, V.V., Krylov, I.K., Mamonov, V.I. (2018). Properties and destruction of anisotropic composite materials under static deformation and impact loading conditions. Journal of Physics: Conference Series, 1134(1): 012028. https://doi.org/10.1088/1742-6596/1134/1/012028
[27] Callister, W.D. (2003). Materials science and engineering an introduction. Sixth Edition, John Wiley and Sons, Inc.
[28] Vijaya Ramnath, B., Rajesh, S., Elanchezhian, C., Santosh Shankar, A., Pithchai Pandian, S., Vickneshwaran, S., Sundar Rajan, R. (2016). Investigation on mechanical behaviour of twisted natural fiber hybrid composite fabricated by vacuum assisted compression molding technique. Fibers and Polymers, 17: 80-87. https://doi.org/10.1007/s12221-016-5276-7
[29] Prabhu, L., Krishnaraj, V., Sathish, S., Sathyamoorthy, V. (2017). Experimental and finite element analysis of

GFRP composite laminates with combined bolted and bonded joints. Indian Journal of Science and Technology, 10(14): 1-7. https://doi.org/10.17485/ijst/2017/v10i14/104606

[30] Al-Sarraj, G.I., Ahmed, S.H., Mohammed, S.A. (2023). Studying the bending behavior of polymer-based composites reinforced with wires of different geometric shapes by numerical analysis method. SVU-International Journal of Engineering Sciences and Applications, 4(2): 209-215. https://doi.org/10.21608/svusrc.2023.199089.1115

[31] AL-Hassani, E.S., Areef, S.R. (2010). The effect of fiber orientation on creep behavior and flextural strength in epoxy composites. Engineering & Technology Journal, 28(7): 1281-1289. https://www.researchgate.net/publication/267233539.